Journal of Physics D: Applied Physics

PAPER

Enhancing light absorption in a thin film silicon tandem solar cell fabricated on a reactive ion etched nano-structured glass surface

To cite this article: Shihyun Ahn *et al* 2019 *J. Phys. D: Appl. Phys.* **52** 035502

IOP Publishing | Journal of Physics D: Applied Physics

J. Phys. D: Appl. Phys. **52** (2019) 035502 (11pp) https://doi.org/10.1088/1361-6463/aaebe6

Enhancing light absorption in a thin film silicon tandem solar cell fabricated on a reactive ion etched nano-structured glass surface

Shihyun Ahn[1,2], S M Iftiquar[1,6], Jaehyun Cho[1], Anh Huy Tuan Le[1], Cheolmin Park[3], Jinjoo Park[1], Hyunhwa Lee[2], Keunkee Hong[4], Jung Soo Kim[1], Sungjae Bong[5] and Junsin Yi[1,6]

[1] College of Information and Communications Engineering, Sungkyunkwan University, 2066, Seobu-ro, Jangan-gu, Suwon-si, Gyeonggi-do, 16419, Republic of Korea

[2] Research Laboratory of Renewable Energy, Hanvit D&S Co., Ltd, 301, 551-17, Yangcheon-ro, Gangseo-gu, Seoul, 07532, Republic of Korea

[3] Department of Energy Science, Sungkyunkwan University, 300 Chunchun-dong, Jangan-gu, Suwon, Gyeonggi-do 440-746, Republic of Korea

[4] Solar cell R&D team, R&D Center, Shinsung E&G Co., Ltd, Daewangpangyo-ro 395, Bundang-gu, Seongnam-si, Gyeonggi-do, 13543, Republic of Korea

[5] Laser Advanced System Industrialization Center, Jeonnam Technopark, Nanosandan 5-ro, 60-7, Nam-myeon, Jangseong-gun, Jeollannam-do, 57248, Republic of Korea

E-mail: junsin@skku.edu and iftiquar@skku.edu

Received 11 July 2018, revised 16 October 2018
Accepted for publication 26 October 2018
Published 14 November 2018

Abstract

The efficient capture and absorption of light are important aspects in improving the photovoltaic conversion efficiency of a solar cell. In a two-terminal tandem device, the output current density is limited by the lowest current-generating component sub-cell. We attempted by experiment to improve the current density of both sub-cells, using an inverted pyramid-type textured glass substrate. One of the two surfaces of the glass substrates was textured by semi-anisotropic reactive ion etching (RIE) with a 100 sccm flow rate of SF_6 gas, and with 7 μm × 7 μm square-shaped etch masks, and obtained an optimum texture of base dimension ~7 μm, height ~8.5 μm, tip diameter ~75 nm and tip to tip separation between neighboring pyramids were about 9 μm. Tandem solar cells that were fabricated on these textured surfaces receive light from the base of these micro-pyramids, thereby enhancing light absorption in the active layers of the device. The shape of the texture and orientation of layers of the tandem solar cell ensured a longer optical path inside the solar cell, leading to higher optical absorption and an improvement in device performance. We observed an increase in the short circuit current density from 11.52 to 14.30 mA cm^{-2}, and in the device efficiency from 11.97% to 14.22%.

Keywords: pyramidal surface texture, tandem solar cell, light trapping, broad band light capture, current density, power conversion efficiency

(Some figures may appear in colour only in the online journal)

[6] Authors to whom any correspondence should be addressed.

1. Introduction

The light intensity inside a textured non-absorbing thin layer can be enhanced by light trapping and multiple internal reflections [1]. In an absorbing medium, the overall optical absorption is also expected to increase with the help of multiple internal reflections or light trapping. Another important aspect of light management in a solar cell is to efficiently capture the incident light. This is popularly achieved with the help of a textured surface [2–7], among which a nano-cone type surface texture [7, 8] or a combination of surface texture and anti-reflection layer [9] are helpful. The textured front surface was demonstrated in a single junction type [2–5, 8, 10, 11], as well as tandem solar cells [12–17], but details of the mechanisms of improvement are limited. In addition to the nano-cone, an inverted pyramid structure [18–20] is also one of the most popular shapes of surface texture. It is well known that a two-terminal tandem solar cell is current-limited by the lowest current-generating sub-cell [21, 22]. Therefore, in a tandem cell, light trapping can be another useful approach to enhance the current density of both sub-cells so that the overall current density of the device can be improved.

One of the approaches is to modify the inner surface of a glass substrate, and deposit the solar cell of the textured surface. It was reported that submicron surface texturing shows an improvement in efficiency of a-Si/mc-Si tandem solar cells by about 1% [14]. Two dimensionally periodic transparent conducting layers show an improvement in device efficiency from 6.9% to 10.0% [15]. An amorphous silicon/c-Si tandem cell with nano-pyramidal texturing of the front surface shows an improvement in power conversion efficiency (PCE) from 10.3% to 13.3% [16]. Texturing the front electrode with a pulsed laser interference technique also leads to an improvement in J_{sc} from 9.2 to 11.2 mA cm^{-2}, and an improvement in device efficiency from 10.2% to 11.5% [17]. These results indicate that a significant improvement in device efficiency is possible by texturing the inner surface of a glass substrate and depositing the solar cell on the textured surface.

Inductively coupled plasma (ICP) reactive ion etching (RIE) is a popular method to create a high aspect ratio surface texture [23]. It is efficient in reproducing an image of a mask. This is done by a suitable anisotropic etching [24, 25]. Isotropic etching is also possible in ICP RIE [26], especially when the density of neutral radicals is higher. In the formation of a 3D pyramid structure, a combination of anisotropic and isotropic etching is necessary. Similar pyramid structures were also reported with multi-crystalline silicon [27], but here our work is based on fabricating thin film silicon tandem solar cells on inverted pyramid-shaped textured glass. Two-terminal tandem solar cells usually have a lower current density as optical spectra is divided among the sub-cells and output current density is limited by the lowest current-generating sub-cell. Therefore, raising the current density (J) is one of the most important requirements to improve device efficiency. Here, we used light trapping with a textured surface to improve J. We prepared the textured surface, fabricated tandem solar cells, investigated device characteristics, and found that a highly textured glass surface can result in high device efficiency. This is not only because of light trapping with the textured surface, but is also due to the orientation of layers of the solar cell, whereby total optical path length increases significantly, leading to an increased optical absorption, quantum efficiency, current density and device efficiency.

2. Experimental

2.1. Dry etching

We used borosilicate glass as a superstrate window of the tandem solar cell and textured one of its two surfaces by using the ICP RIE, where SF_6 etchant gas was used, with a 100 sccm flow rate and with various plasma conditions. Etch masks were fabricated on the glass surface by using a 7 μm $\times$ 7 μm square shaped photolithographic (PL) mask. Each square etch mask was separated by 2 μm, from edge to edge. The glasses were 5 cm $\times$ 5 cm in size. Initially, the glass was cleaned with acetone, methanol, and deionized water (DIW). Then a 700 nm thick Al layer was deposited by thermal evaporation as a hard mask. After that, the surface was coated with positive photo resist (PR). In the PL process, the surface was covered with the PL mask and exposed to ultra-violet (UV) light. Then it was wet-etched in a solution of HNO_3: CH_3COOH: H_3PO_4: H_2O at a volume ratio of 4:3.5:73:19.5, at 25 °C. This resulted in the removal of PR and Al from the UV-exposed area. Then the glass was cleaned further with acetone, methanol, and DIW. After that the ICP RIE dry etching was performed with SF_6 gas in the 13.56 MHz radio frequency (RF) plasma.

The RIE was carried out at room temperature. Our preliminary investigation shows that 100 to 300 W RF bias power and with the ICP power in the range of 600 to 1000 W can provide good etching. We also varied the gas pressure from 10 mTorr to 40 mTorr. A higher ICP source power can give higher plasma density, while increasing the bias power can lead to higher energy of the bombarding etchant ions. As reported in the literature, we also observed that by raising either or both the powers [28, 29] resulted in a higher etching rate [30], while raising the ICP power and/or gas pressure [31] leads to an increase in the etching rate as well as the undercut [32] in the masked area.

2.2. Device fabrication

Tandem structured thin film silicon solar cell devices were fabricated on these textured glasses. The glasses were coated with an Al-doped zinc oxide (AZO) double layer by DC magnetron sputtering as follows. The first AZO layer (the seed layer, of 100 nm thickness) was deposited at 100 W power, 12 mTorr pressure, 20 sccm Ar flow, with a substrate temperature (T_s) of 270 °C. Then the second AZO layer (the main layer, of 700 nm thickness) was deposited with 300 W power, 12 mTorr pressure, 20 sccm Ar gas flow, and with a T_s of 270 °C. In order to nano-texturize the AZO surface it was treated with DIW:HCl:oxalic acid at a volume ratio of 245:4:125, at 25 °C, for 10 s. Solar cell layers were then deposited in a cluster type multi-chamber radio frequency plasma enhanced chemical vapor deposition (RF PECVD)

Table 1. Deposition conditions for the various silicon alloy layers of the tandem solar cell in the RF PECVD system. The deposition conditions are given as SiH_4:H_2:CO_2:dopant-gas/pressure/RF power/T_s/electrode distance of RF PECVD system. In cases of p-type double-layers [33, 34] (p1 and p2), diborane (B_2H_6) was used as dopant gas, and in cases of n-type layers (i/n buffer and n-layer), phosphine (PH_3) was used as dopant gas. For intrinsic and n-type layers, CO_2 gas was absent, while for the intrinsic layers the dopant gases were also absent. Here, *d* denotes thickness, and p-nc-SiO:H, p-a-SiO:H, and p-nc-Si:H indicate respectively the p-type nano-crystalline silicon oxide, p-type amorphous silicon oxide, and p-type nano-crystalline silicon. Further, the i-a-Si:H and i-nc-Si:H indicate intrinsic amorphous silicon and nano-crystalline silicon, respectively, and the n-nc-Si:H, n-a-Si:H indicate n-type nano-crystalline silicon, amorphous silicon, respectively.

Sub-cell	Electrode	p2-layer	p1-layer	Seed layer	i-layer	i/n buffer	n-layer	Electrode
Top	AZO	d = 20 nm, p-nc-SiO:H 5:900:2.1:3 $\times$ 10^{-3}/1.5 torr/20 W /100 °C/20 mm	d = 25 nm, p-a-SiO:H 5:500:10:1 $\times$ 10^{-2}/1.5 torr/20 W/100 °C/20 mm	Absent	d = 450 nm, i-a-Si:H 10:40/1.5 torr/20 W/180 °C/20 mm	Absent	d = 50 nm n- nc-Si:H 3:300:0.08/1.5 torr/100 W/180 °C/20 mm	Absent
Bottom		Absent	d = 30 nm p-nc-Si:H 5:800:3 $\times$ 10^{-3}/1.5 torr/300 W /200 °C/20 mm	d = 60 nm i-nc-Si:H 3:600 /1.5 torr/100 W /200 °C/15 mm	d = 3500 nm i-nc-Si:H 3:150/3 torr/150 W/200 °C/15 mm	d = 10 nm n-a-Si:H 30:120:30 /0.2 torr/500 W/180 °C/20 mm	d = 50 nm n-nc-Si:H 3:300:8/1.5 torr/100 W /180 °C/20 mm	AZO

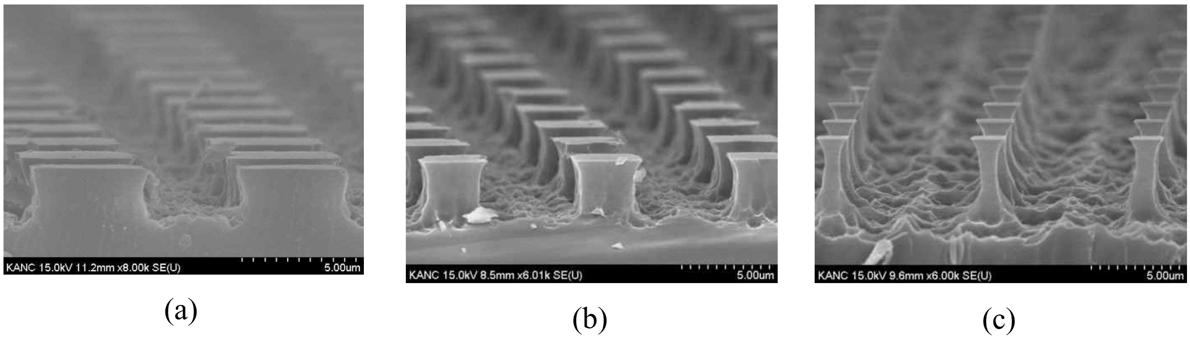

Figure 1. SEM image of etched glass surface, etched for 150 min, with 1000 W ICP, 300 W bias power, no argon gas flow but with chamber pressure (a) 10 mTorr, (b) 20 mTorr, and (c) 40 mTorr.

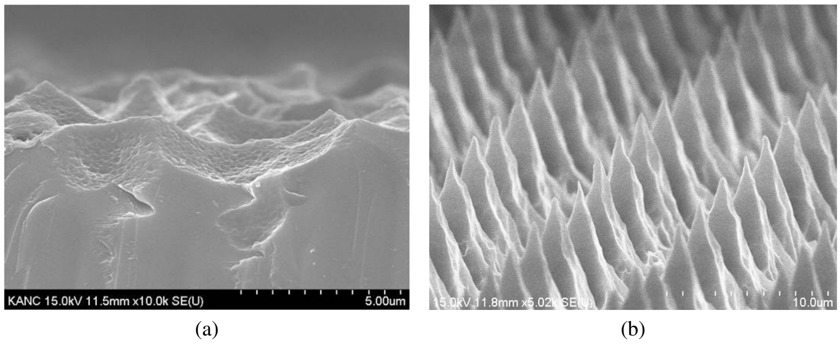

Figure 2. SEM image of two of the types of glass surface used in fabricating the solar cells. (a) Low surface roughness of textured glass, due to excess etching time, AR-1. (b) High surface roughness of textured glass, AR-3.

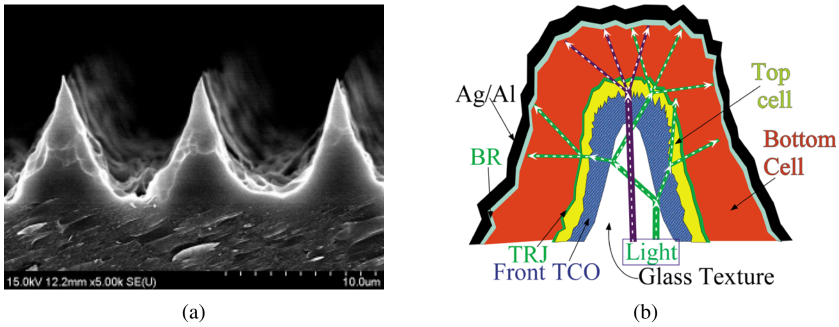

Figure 3. (a) SEM image of glass texture obtained by ICP RIE, with tip diameter 50–100 nm. (b) Schematic diagram of cross-section of tandem solar cell fabricated on pyramid-shaped glass texture. BR: back reflector [22]. TCO: transparent conducting oxide (AZO). TRJ: tunnel-recombination junction [35].

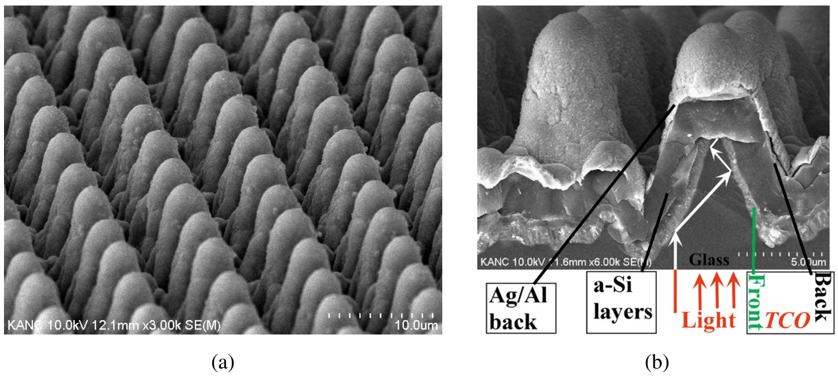

Figure 4. (a) Bottom view SEM image of the tandem solar cell, fabricated on a textured glass. Here the visible surface is an Ag/Al layer, as per figure 3(c). (b) Cross-sectional SEM image of the tandem solar cell. Here the different layers are labeled for further clarity.

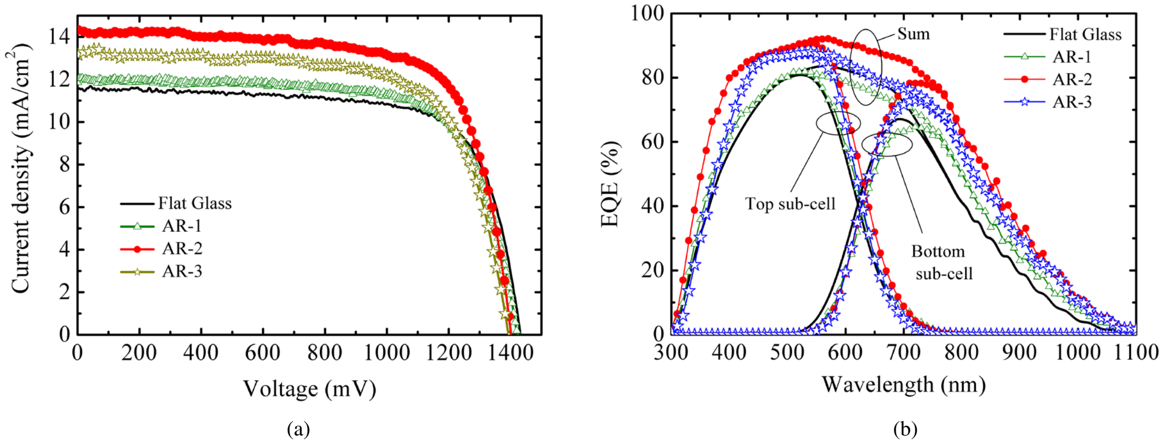

Figure 5. Experimental results of: (a) J–V characteristic curves; (b) EQE spectra of the tandem solar cells. The black continuous lines are for cells fabricated on a flat surface (Cell-1), while the curves with marked symbols are for the cells fabricated on the pyramid-shaped surface structures (Cells-2, 3, 4, as indicated in table 2).

Table 2. Extracted parameters of the tandem solar cells, as obtained from figure 5(a).

Substrate type (cell)	V_{oc} (mV)	J_{sc} (mA cm^{-2})	FF (%)	Efficiency (%)
Flat glass (Cell-1)	1432.3	11.52	72.6	11.97
AR-1 (Cell-2)	1422.6	11.96	71.5	12.16
AR-2 (Cell-3)	1402.0	14.30	70.9	14.22
AR-3 (Cell-4)	1394.0	13.27	69.1	12.78

Table 3. Capability of producing J_{sc} independently by the top sub-cell (J_{sc1}) and bottom sub-cell (J_{sc2}), obtained by integrating the respective EQE spectra shown in figure 5(b).

Substrate type	J_{sc1} (mA cm^{-2})	J_{sc2} (mA cm^{-2})	Experimental J_{sc} (mA cm^{-2})
Flat glass	14.51	11.52	11.52
AR-1	15.18	11.96	11.96
AR-2	17.61	14.30	14.30
AR-3	15.49	13.27	13.27

system. The deposition conditions are given in table 1. Our investigation was primarily based on the effects of light trapping on a tandem solar cell. This was tested by using differently textured glass surfaces. Therefore, deposition conditions and the specifics of the layers of the tandem solar cell were kept unchanged. We obtained different texturing of the glass surfaces, and therefore, the performances of tandem solar cells under AM1.5G insolation varied because of the differences obtained with the differently textured glass surfaces.

Scanning electron microscopic (SEM) images were taken of the surfaces of textured bare glass, surfaces with the fabricated device, and cross-sectional views of the cells. AM1.5G insolation was used for measuring current density voltage (J–V) characteristic curves, while wavelength-dependent external quantum efficiency (EQE) was measured with an EQE instrument (model QEX7; PV Measurements, Inc.).

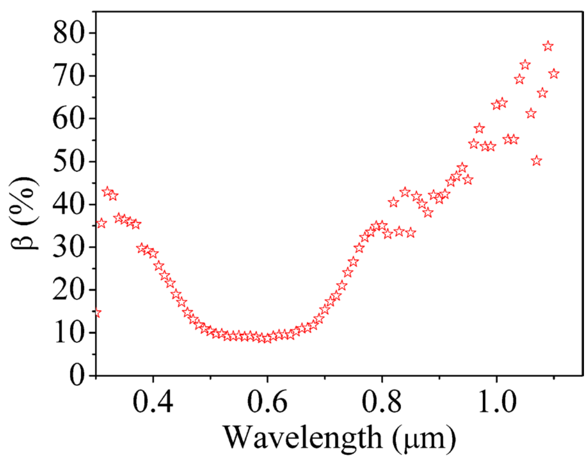

Figure 6. Wavelength-dependent EQE enhancement factor of Cell-2, with reference to Cell-1.

3. Results

3.1. Dry etching

Our investigation shows that the desired etching of the glass surface is achievable within 100 to 300 W RF bias power, with the ICP power in the range of 600 to 1000 W and with a gas pressure of 10 mTorr to 40 mTorr.

Figure 1 shows the evolution of the undercut that we observed with the increase in chamber pressure. At a lower ICP power, the undercut is reduced. In our plasma etching, 600 W of ICP power gave us suitable etched surfaces. We also used Ar gas dilution that reduces the etching rate as well as the undercut.

Figure 2 shows SEM surface images of two of the types of glasses used in fabricating the solar cells. Figure 2(a) shows the lower surface roughness that was obtained due to excess ion etching of the glass surface, where the pyramidal structures were damaged due to a relatively higher etching rate. The surface in figure 2(a) was obtained with 600 W ICP power, 300 W bias power, 20 mTorr pressure and 150 min of etching with a 100 sccm flow rate of SF_6, while the structure

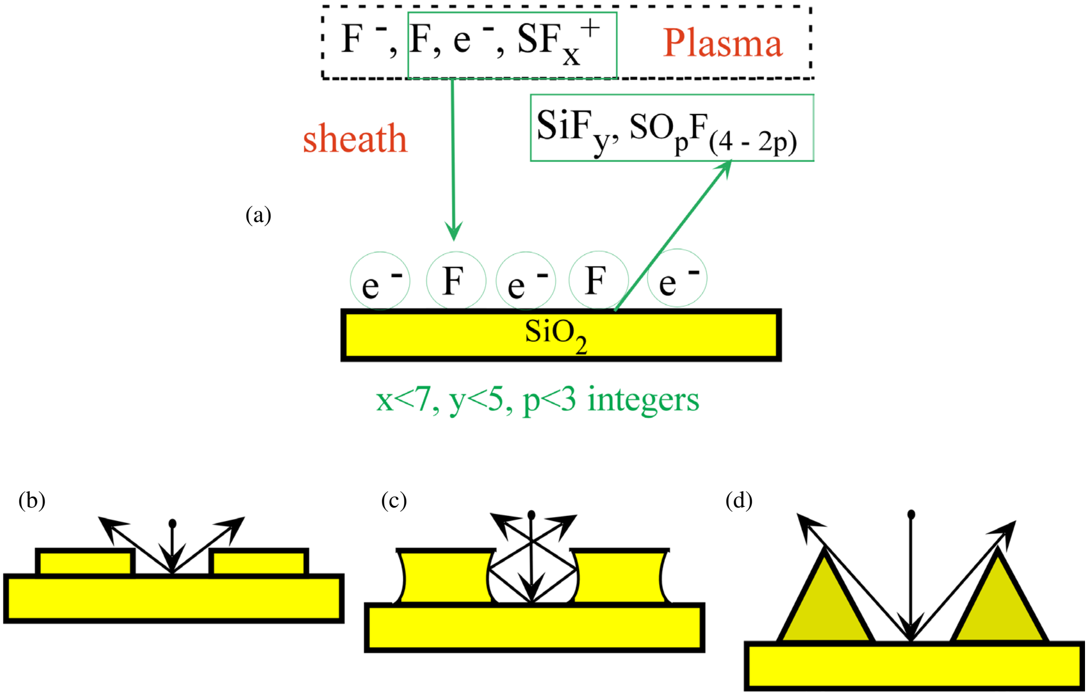

Figure 7. Schematic diagram showing mechanism of evolution of pyramid-shaped surface structure due to semi-anisotropic etching in ICP RIE. (a) Expected plasma process; (b) start of anisotropic etching; (c) sputtering induced and isotropic etching of side wall of texture, and (d) final pyramid-shaped surface texture.

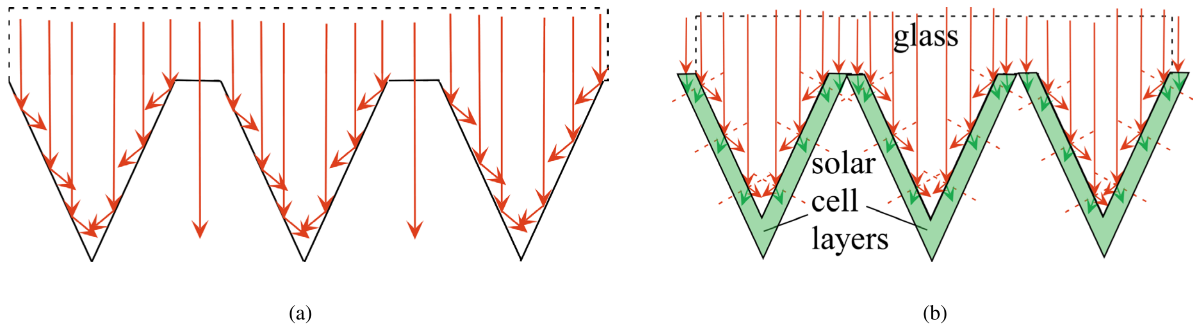

Figure 8. Ray diagram of effective light trapping, (a) in textured glass, where light faces total internal reflection on the inverted pyramidal structure while light transmits through the flat region, (b) in solar cell deposited on the textured glass, where all the light is effectively collected by the solar cell layers, leading to a far longer optical path length within the cell.

of figure 2(b) was obtained with the same conditions as those of figure 2(a) except with 10 mTorr chamber pressure.

Figure 3(a) shows an SEM image of one of the plasma etched surface structures, obtained with similar conditions as those of figure 2(a) but at 15 mTorr pressure. Here, the tips of the pyramids were 50 to 100 nm in diameter, while base widths were ~7 μm and the height of the pyramids was ~8.5 μm. In solar cell applications, light enters from the base of the pyramids. It can be called a high aspect ratio surface texture (AR-2). Here, the term 'AR' is used to indicate aspect ratio; that is, the ratio between the height and width of a texture. A higher aspect ratio indicates a sharper surface texture and higher surface roughness. A schematic diagram of application of such a surface structure is shown in figure 3(b).

3.2. Tandem solar cell on textured glass

Figure 4(a) shows SEM images of the back side or bottom view of the solar cells on the glass texture that was covered with Ag/Al layers. The Ag/Al layer acts as a metal contact negative electrode of the solar cells, while the positive electrode is the front TCO, as shown in the schematic diagram, figure 3(b).

Solar cells generate electrical power from sunlight. The output power can be scaled based on the PCE. This PCE was estimated from the *J–V* characteristic curves. These curves are shown in figure 5(a). Figure 5(b) shows the EQE spectra. The primary purpose of using a textured glass surface for a solar cell is to achieve an enhanced light capture. Reduced reflection or higher optical transmission is an indication of enhancement of light capture. It can be expressed by equation (1) [4]:

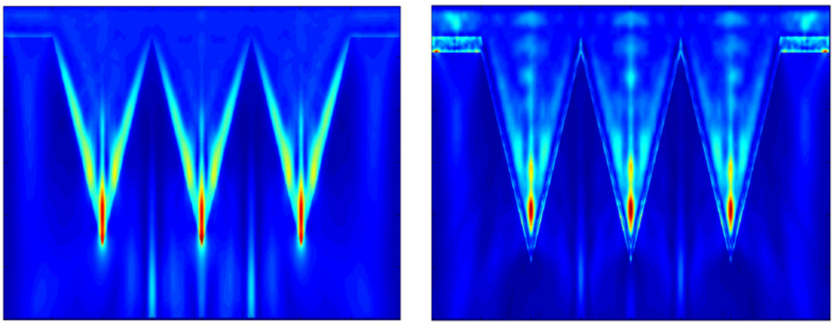

(a) (b)

Figure 9. Finite difference time domain (FDTD) simulation of passage of white light through an inverted pyramidal glass surface: (a) without solar cell deposited on it; (b) with solar cell deposited on it. The color bar indicates light intensity in arbitrary units. Here, we assumed all the layers are non-absorbing of light.

$$I_T = I_0\left(1 - R^x\right). \quad (1)$$

Here, x indicates the number of times a ray hits a pyramid structure before traveling towards infinity, I_T is the transmitted light and I_0 is the incident light intensity, and R is reflectivity. The short circuit current density (J_{sc}) can be expressed as

$$J_{sc} = K_a \cdot \int_{l1}^{l2} I_T \, dl = K_a \cdot I_0 \int_{l1}^{l2} \left(1 - R^x\right) \, dl \quad (2)$$

where the integration is from wavelength l_1 to l_2, dl is the differential of the wavelength, and the constant term K_a is related to IQE, parasitic absorption and internal reflection at the interfaces of the layers. In the case of our textured surface, $x > 1$, while for a flat surface, $x = 1$. In order to indicate that the J_{sc} is directly related to the light capture, a simplified form of the J_{sc} is given in equation (2). According to classical ray optical formalism [3–5], it can be said that x should be higher for better light capture or reduced reflection loss of incident light.

The solar cell parameters extracted from figure 5(a) are shown in table 2. It shows that the performance of tandem solar cells fabricated on textured surfaces, remain better than those with a flat glass substrate. Both J_{sc} and device efficiency increased from the flat cell (Cell-1) to Cell-3, that is with AR-2, although J_{sc} and PCE decreased from Cell-3 to Cell-4. Furthermore, it can be seen that the V_{oc} and FF of the tandem cells remain highest for Cell-1, that was fabricated on a flat substrate, and both of these parameters steadily decreased from Cell-1 to Cell-4. Table 3 shows the current producing capability of the two sub-cells of the tandem solar cells. These are obtained by spectral integration of the EQE spectra, and normalizing with the output current density. Figure 5(b) and table 3 show that the bottom cell is the current-limiting sub-cell, and that the device structure is not optimized, as indicated by J_{sc1} and J_{sc2} being different. However, the EQE spectra also indicates that Cell-3 or the substrate AR-2 was demonstrating the best results in its device application.

Therefore, the textured surface AR-2 is expected to deliver more light to the solar cells than the flat surface. Experimentally, we observed an enhanced J_{sc} of the tandem solar cell that increased from 11.52 to 14.30 mA cm^{-2}; it can be considered as an effect of improved light coupling to the

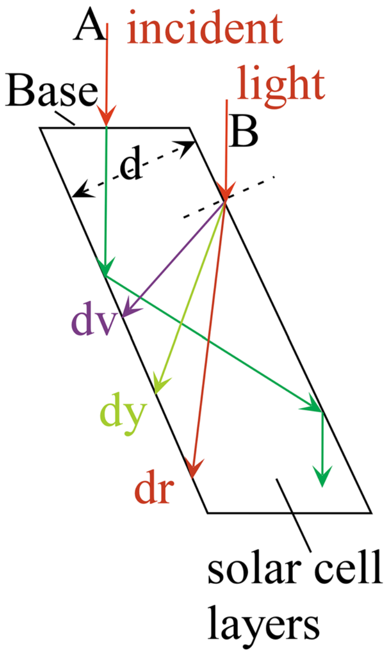

Figure 10. Schematic demonstration of light ray passing through inclined solar cell. Here, d is the thickness of the solar cell, dv, dy, and dr are the geometric lengths within the solar cells covered by violet, yellow, and red lights. 'Base' indicates the base of the pyramidal texture. Rays 'A' and 'B' contribute to EQE enhancement, as discussed later using equations (5) and (6).

active layers of the cell. Absorbed light in the active layer generates energetic electron–hole pairs that contribute to output current. Therefore, one estimation of light coupling to the active layer of the bottom sub-cell (as the bottom sub-cell remains the current-limiting cell) can be made by estimating the J_{sc} enhancement factor, which we can call α, by using expression (3):

$$\alpha = \frac{\left(J_{sc2(b)} - J_{sc2(a)}\right)}{J_{sc2(a)}}. \quad (3)$$

Here the subscript (a) indicates the J_{sc2} for Cell-1, while the subscript (b) indicates the J_{sc2} for any other cells (Cell-2, 3, 4) Another indication of improved light trapping is the EQE spectra. When wavelength-dependent short circuit current density is measured, it gives wavelength-specific characteristics of photo-induced response or the overall effect of light trapping. We experimentally obtained the EQE spectra, as shown in figure 5(b). The wavelength-dependent EQE enhancement factor, say β, can be obtained from expression (4) and is shown in figure 6. Here EQE_1 is the 'Sum'-EQE spectra for Cell-1, as shown in figure 5(b), while EQE_2 is the 'Sum'-EQE spectra for any of the other cells.

$$\beta = \frac{(EQE_2 - EQE_1\ )}{EQE_1}. \tag{4}$$

4. Discussion

Usually, ICP RIE is used to transfer the image of a mask to a substrate, by anisotropic RIE [24] and with SF_6 as the etchant [23, 36, 37]. It is used for a certain degree of isotropic etching as well [26, 38, 39], as a result of which undercut develops. As our preferred shape of surface structure was a pyramid type, so we combined the isotropic with anisotropic etching or a semi-anisotropic etching.

Etching by electrically neutral radicals is isotropic, and these neutral radicals are abundant in a plasma for its longer lifetime, density of which increases with an increased ICP power and also chamber pressure. We obtained the pyramid-shaped textures with a 600 W ICP source power, 300 W bias power, at 10 to 20 mTorr pressure and 2 h of etching.

4.1. Etching mechanism

The plasma was generated by the collisions between the electrons and SF_6. SF_6 can break into SF_p radicals that can easily become positively charged ions, where integer $p < 6$. The $(6 - p)$ number of F atoms that are broken off from the SF_6, may become charged or may remain neutral. These F^- ions or F radicals will then react with Si of the glass [40], converting SiO_2 to SiF_4 and afterwards leaving the chamber, while oxygen of the SiO_2 can react with SF_p, forming SO_2 or SOF_q $(1 < q < 4)$, and can also leave the chamber [25]. The undercut may develop because of the isotropic etching of the F radicals. Formation of the pyramid structure is schematically demonstrated in figure 7.

4.2. Light trapping

Tandem solar cells fabricated on these pyramidally textured surfaces show improved performance, and the reason for the improvement is known as light trapping. It is to be noted that the EQE enhancement factor, as shown in figure 6, is significantly larger than the optical reflectivity of one of the two surfaces of the glass. This means that if only reduced optical reflectivity and back reflection are considered to be responsible for the enhanced performance of the tandem solar cells, then the experimentally measured enhancement is more than what is expected. In order to explain the unusually high gain in β, we give the following explanations. The active wavelength range of a thin film silicon solar cell is approximately from 300 nm to 1000 nm. As the texture base is of 7 μm $\times$ 7 μm square shape, which is significantly larger than the wavelength of light, the classical ray optics can be used in the whole range of spectra. Light passes through the base of the pyramids and then travels towards its apex.

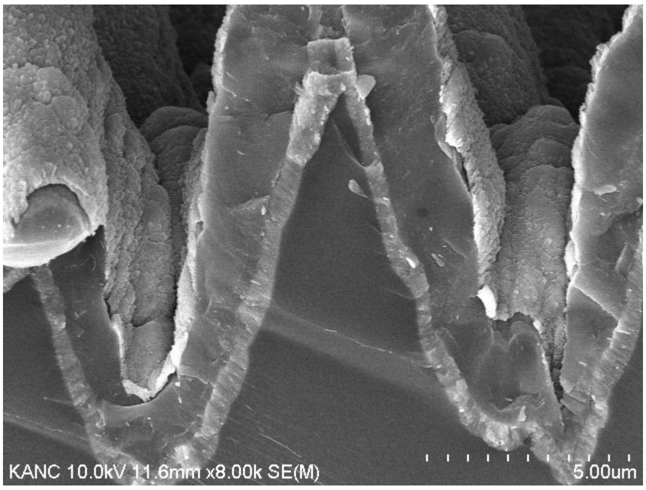

Figure 11. Cross-sectional SEM image of cell fabricated on AR-3 type substrate.

The angle of the surface texture, as shown in figure 3(a), is such that the vertically incident light will have total internal reflection (TIR) at the glass–air interface, as shown schematically in figure 8(a). However, in the presence of layers of the solar cell, whose refractive index is comparable to or higher than that of the glass, TIR will not take place and the light will enter the layers of the cell, as schematically demonstrated in figure 8(b).

This situation was also observed in a finite difference time domain simulation. We used it to investigate the total internal reflection of light within the inverted pyramidal glass texture and then the passing of light to solar cell layers. Therefore, measuring the transmission of light through textured glass will be inaccurate, as light will not transmit to air from glass (figure 9(a)) but will transmit to the solar cell layers (figure 9(b)).

When light enters through the base of pyramids [10], these glass structures act as a light funnel. Within the pyramids the light faces TIR, while at the flat intermediate surfaces between the pyramids light is transmitted, as schematically shown in figure 8(a). But when solar cell layers are deposited on these structures, the TIR at the glass surface disappears because the air medium is now replaced by solar cell layers. This ensures optical transmittance from a rarer glass medium to a denser solar cell. In cases of solar cells fabricated on a flat surface, light travels perpendicular to the surface and therefore the effective optical thicknesses of the layers are nd, where n is the refractive index and d is the thickness of the layer. On the other hand, when a solar cell is deposited on a textured surface, the inclined planes of the pyramids ensure that incident light travels a longer distance within each of the active layers of the tandem cell. The refractive indices of the amorphous silicon layers vary with wavelength, which is generally larger

(~5) in shorter wavelengths and smaller (~3) in longer wavelengths, leading to an angular dispersion of transmitted light, demonstrated schematically in figure 10, where d is the actual thickness of film, and dv, dy, and dr are the representative geometric path lengths traveled by violet, yellow and red lights, respectively, with $dv < dy < dr$. The absorption coefficient for a shorter wavelength light is higher than that of a longer wavelength. Therefore, overall optical absorption in a textured solar cell will be higher than that in a non-textured one. From figure 10, it becomes clear that the effective geometric length of the path followed by light is significantly larger for the cells deposited on the textured surface than those on a flat surface. The effect can be visible in the EQE spectra, as shown in figure 5(b).

Considering ray optics, it can be estimated that in a multiple internal reflection, more light is absorbed to the cell. For example, if the incident light hits the internal surface of the pyramids x times, then the intensity of transmitted light will be $I_T = I_0(1 - R^x)$, as $R < 1$ therefore $I_T \approx I_0$ when x is larger. This can be achieved in a high aspect ratio pyramid-type surface structure.

Based on [5], the EQE of the component sub-cells can be expressed as

$$\mathrm{EQE}_{\lambda 1} = (1 - R_F)(1 - k_{TCO})(1 - k_{p1})\left[k_{i1}(1 + \Phi_{t1}) + k'_{i1}\right] \tag{5}$$

$$\mathrm{EQE}_{\lambda 2} = T_1(1 - k_{p2})\left[k_{i2}(1 + \Phi_{t2}) + k'_{i2}\right]. \tag{6}$$

Here, equation (5) corresponds to the wavelength-dependent EQE of the top sub-cell and equation (6) corresponds to that of the bottom cell, R_F is the reflectivity of the top surface, and Φ_{t1} is the EQE enhancement factor due to light trapping by internal reflections (a contribution that is coming from rays of type 'B' in figure 10). Further, k_{TCO} is the absorbance of front TCO, k_{p1} and k_{i1} are the absorbances of the p-layer and i-layer of the front sub-cell when light travels in a direction near-normal to the local interfaces, while k'_{i1} is the optical absorbance of light in the i-layer of the top cell when the geometric path length of light is longer than the layer thickness (a contribution coming from rays of type 'A', as indicated in figure 10). Similarly, the terms in equation (6) correspond with the '2' in subscript indicating the bottom sub-cell, and T_1 indicating optical transmittance through the top sub-cell. Here, k'_{i1} and k'_{i2} are two additional terms that arise due to the unusually long path length of light as indicated by the rays of type 'A' in figure 10. These two terms contribute to a significant enhancement in the EQE spectra in figure 5(b). Here, the terms Φ_{t1}, Φ_{t2} are due to back reflection or internal reflection of light, while the terms k'_{i1}, k'_{i2} are the EQE enhancement due to the prolonged optical path length within the active layers with or without back reflection or internal reflection. Both these terms contribute to the EQE enhancement factor β.

Therefore, due to the effective lengthening of the geometric path of incident light and light funneling at the textured surface, the EQE enhancement factor, β (figure 6), shows a high value.

Furthermore, it can be seen from the J–V characteristic curves that the V_{oc} values of the tandem solar cells fabricated on textured surfaces are lower than those on flat glass. This is possibly because of local shunting of currents in a non-uniform solar cell [41]. In a non-uniform solar cell, the output voltage changes because of thickness variation, as demonstrated in [41]. This leads to local shunting of currents, as a result of which the V_{oc} of Cells-2, 3, 4 were observed to be lower than that on flat glass (Cell-1). The small non-uniformity in thickness of the cell layers can also be noticed in the SEM image of the cross-section of the cell. This non-uniformity is primarily because of plasma deposition of the silicon layers, where fewer radicals will reach the bottom of the pyramids than towards the top of the pyramids, thereby making the silicon layers thinner towards the base of the pyramids than around its apex. Figure 11 shows a cross-sectional SEM image of Cell-4, deposited on an AR-3 superstrate. Here, the difference in thickness of cell layers between the tip and base of the pyramid is prominent. The significantly thinner cell layers at the base can lead to a reduced device performance. Although variations in layer thickness of the solar cell and non-uniform distribution of light intensity may compensate to some extent, a significant difference in the thickness of the cell layers over the pyramids can reduce the overall device efficiency.

This non-uniformity can be reduced in a suitable plasma condition, where more SiH_3 radicals are generated [42]. Furthermore, any periodic surface structure [43–45] is prone to exhibit wavelength-dependent diffraction, scattering and/or reflection. But in our design, these effects are expected to be low.

4.3. Comparison of results

Our experimental results show an improvement in efficiency of a tandem solar cell when it was fabricated on a textured glass, in comparison to a cell fabricated on a non-textured glass surface. We obtained a maximum improvement in PCE of 2.25 percentage points, from 11.97% to 14.22%, with ~ 7 μm base width and ~8.5 μm high pyramidal textures, while J_{sc} of our cells improved from 11.52 to 14.34 mA cm^{-2}. Earlier reported results show an improvement of ~1.0% in PCE of a-Si/mc-Si tandem solar cells when a hemi-spherical texture was used and where the sizes of the textures were within a range of 500 nm to 2500 nm [14]. A 1000 nm periodic 2D grating structure of front TCO leads to an improvement in device efficiency of 3.1 percentage points, from 6.9% to 10.0% [15]. Here, the EQE spectra in the longer wavelength region shows a significant improvement but in the shorter wavelength region EQE was reduced, probably because of increased optical absorption in the 2D gratings structure, as reported in [15]. An inverted nano-pyramid structure, obtained by texturing a c-Si wafer and then depositing a a-Si top cell, resulted in an improvement in J_{sc} from 9.6 to 13.4 mA cm^{-2} and in PCE from 10.3% to 13.3% [16]. A hemispherical-shaped periodic texture on a glass surface shows an improvement in PCE from 11.7% to 12.1%, while J_{sc} improved from 11.0 to 12.0 mA cm^{-2} [46]. Ring *et al* reported texturing the front electrode with a pulsed laser interference technique and obtained an improvement in J_{sc} from 9.2 to 11.2 mA cm^{-2}, while PCE improved from

10.2% to 11.5% [17]. A modulated surface texture shows an initial efficiency of a tandem solar cell as 14.8% [47]. All these results show that our results are close to or even better than the reported results, while one major difference in our experiment is that we used a larger sized inverted pyramidal surface texture and obtained a high device efficiency.

5. Conclusions

We have demonstrated that ICP RIE can be used to fabricate pyramid-shaped periodic surface textures, with a high degree of precision, in which the tip diameter can be as small as 50 nm. The shape and size of the texture depends upon etching parameters as well as etching time. These surface structures are useful for effective light trapping in a solar cell over a broad spectral range, thereby raising its current density and overall enhancement in EQE. A flat glass surface has a higher reflectivity in the shorter as well as in the longer wavelength region that can be significantly reduced by using an inverted pyramidal surface texture. Tandem-structured silicon thin film solar cells were deposited on this textured surface so that the pyramids act as light funnels, and the geometric path length of light increases over the inclined films deposited at the surface of the inverted pyramids. As a result, it raises J_{sc} from 11.52 to 14.34 mA cm^{-2} and we obtained a device efficiency of 14.22%. The EQE and J-V characteristic curves show that an overall improvement in device performance was obtained with these surface textures. As the deposition conditions of the layers of the tandem solar cells were kept unchanged, a significant improvement in device performance was observed from the flat surface to the optimized surface texture. An increase in the size of the pyramids beyond the optimum size may lead to a non-uniform deposition of subsequent layers of the solar cell, leading to a decrease in the device performance. This indicates that a further optimization of the deposition conditions of the cell layers is required – an optimized condition that is suitable for the textured surface. In this way the device efficiency can be further improved for the substrate type AR-3.

Acknowledgments

This research was supported by Individual Research in Basic Science and Engineering through the National Research Foundation of Korea (NRF), funded by the Ministry of Education (NRF-2016R1D1A1B03935259). This work was supported by the New & Renewable Energy Core Technology Program of the Korea Institute of Energy Technology Evaluation and Planning (KETEP), granted financial resource from the Ministry of Trade, Industry & Energy, Republic of Korea (No. 20163010012230).

ORCID iDs

S M Iftiquar https://orcid.org/0000-0002-0135-7760
Jinjoo Park https://orcid.org/0000-0002-6410-0460

References

[1] Yablonovitch E and Cody G D 1982 Intensity enhancement in textured optical sheets for solar cells *IEEE Trans. Electron Devices* **29** 300–5
[2] Campbell P and Green M A 1987 Light trapping properties of pyramidally textured surfaces *J. Appl. Phys.* **62** 243–9
[3] Iftiquar S M, Jang J, Park H, Shin C, Park J, Jung J, Kim S and Yi J 2014 Analysis of optical absorption and quantum efficiency due to light trapping in a n-i-p type amorphous silicon solar cell with textured back reflector *Phys. Status Solidi* a **211** 924–31
[4] Iftiquar S M, Jung J, Park H, Cho J, Shin C, Park J, Jung J, Bong S, Kim S and Yi J 2015 Effect of light trapping in an amorphous silicon solar cell *Thin Solid Films* **587** 117–25
[5] Iftiquar S M, Jung J, Shin C, Park H, Park J, Jung J and Yi J 2015 Light management for enhanced efficiency of textured n-i-p type amorphous silicon solar cell *Sol. Energy Mater. Sol. Cells* **132** 348–55
[6] Choi J, Lee T S, Jeong D S, Lee W S, Kim W M, Lee K S, Kim D and Kim I 2016 Random Si nanopillars for broadband antireflection in crystalline silicon solar cells *J. Phys. D: Appl. Phys.* **49** 375108
[7] Mailoa J P, Lee Y S, Buonassisi T and Kozinsky I 2014 Textured conducting glass by nanosphere lithography for increased light absorption in thin-film solar cells *J. Phys. D: Appl. Phys.* **47** 085105
[8] Zhang D, Ren W, Zhu Z, Zhang H, Liu B, Shi W, Qin X and Cheng C 2015 Highly-ordered silicon inverted nanocone arrays with broadband light antireflectance *Nanoscale Res. Lett.* **10** 9
[9] Kang D W, Lee H M and Han M K 2013 Efficient light incoupling into silicon thin-film solar cells by anti-reflecting MgO/high-compact-AZO with air-side textured glass *J. Phys. D: Appl. Phys.* **46** 485107
[10] Zhao J, Wang A, Campbell P and Green M A 1999 22.7% efficient silicon photovoltaic modules with textured front surface *IEEE Trans. Electron Devices* **46** 1495–7
[11] Wada H, Nishikubo K, Sichanugrist P and Konagai M 2014 Improved light trapping effect for thin-film silicon solar cells fabricated on double-textured white glass substrate *Can. J. Phys.* **92** 920–3
[12] Bessonov A, Cho Y, Jung S J, Park E A, Hwang E S, Lee J W, Shin M and Lee S 2011 Nanoimprint patterning for tunable light trapping in large-area silicon solar cells *Sol. Energy Mater. Sol. Cells* **95** 2886–92
[13] Escarré J, Söderström K, Despeisse M, Nicolay S, Battaglia C, Bugnon G, Ding L, Meillaud F, Haug F J and Ballif C 2012 Geometric light trapping for high efficiency thin film silicon solar cells *Sol. Energy Mater. Sol. Cells* **98** 185–90
[14] He S and Li M 2018 Multi-scale texturing for a-Si/mc-Si thin-film tandem solar cells *AIP Adv.* **8** 035326
[15] Van Erven A J M, Steltenpool M, Rutten J, Van Der Hofstad G, De Groot H, De Ruijter J, Bos M, Titulaer B and Rajeswaran G 2011 Periodically textured glass for 20% bottom cell current increase in a-Si:H/μc-Si:H tandem solar cells *37th IEEE Photovoltaic Specialists Conf., PVSC 2011 (Seattle, WA)* pp 686–9
[16] Li G, Li H, Ho J Y L, Wong M and Kwok H S 2014 Nanopyramid structure for ultrathin c-Si tandem solar cells *Nano Lett.* **14** 2563–8
[17] Ring S, Neubert S, Schultz C, Schmidt S S, Ruske F, Stannowski B, Fink F and Schlatmann R 2015 Light trapping for a-Si: H/μc-Si: H tandem solar cells using direct pulsed laser interference texturing *Phys. Status Solidi* **9** 36–40
[18] Yang L, Liu Y, Wang Y, Chen W, Chen Q, Wu J, Kuznetsov A and Du X 2017 18.87%-efficient inverted pyramid

structured silicon solar cell by one-step Cu-assisted texturization technique *Sol. Energy Mater. Sol. Cells* **166** 121–6

[19] Smith A W and Rohatgi A 1993 Ray tracing analysis of the inverted pyramid texturing geometry for high efficiency silicon solar cells *Sol. Energy Mater. Sol. Cells* **29** 37–49

[20] Tang Q, Shen H, Yao H, Gao K, Jiang Y, Zheng C, Yang W, Li Y, Liu Y and Zhang L 2017 Potential of quasi-inverted pyramid with both efficient light trapping and sufficient wettability for ultrathin c-Si/PEDOT:PSS hybrid solar cells *Sol. Energy Mater. Sol. Cells* **169** 226–35

[21] Iftiquar S M, Lee J C, Lee J, Jang J, Lee Y-J and Yi J 2012 Single- and multiple-junction p-i-n type amorphous silicon solar cells with p-a-$Si_{1-x}C_x$:H and nc-Si:H films *Photodiodes—From Fundamentals to Applications* ed I Yun (Croatia: InTech) pp 289–311

[22] Cho J, Iftiquar S M, Pham D P, Jung J, Park J, Ahn S, Le A H T, Kim J S and Yi J 2017 Improvement in performance of tandem solar cell by applying buffer layer, back reflector and higher crystallinity of the microcrystalline Si active layer of bottom subcell *Thin Solid Films* **639** 56–63

[23] Goyal A, Hood V and Tadigadapa S 2006 High speed anisotropic etching of Pyrex® for microsystems applications *J. Non-Cryst. Solids* **352** 657–63

[24] Akashi T and Yoshimura Y 2006 Deep reactive ion etching of borosilicate glass using an anodically bonded silicon wafer as an etching mask *J. Micromech. Microeng.* **16** 1051–6

[25] Zhang C and Tadigadapa S 2018 Modified inductively coupled plasma reactive ion etch process for high aspect ratio etching of fused silica, borosilicate and aluminosilicate glass substrates *Sensors Actuators* A **273** 147–58

[26] Chen Q, Fang J, Ji H F and Varahramyan K 2008 Isotropic etch for SiO_2 microcantilever release with ICP system *Microelectron. Eng.* **85** 500–7

[27] Park K M, Lee M B and Choi S Y 2015 Investigation of surface features for 17.2% efficiency multi-crystalline silicon solar cells *Sol. Energy Mater. Sol. Cells* **132** 356–62

[28] Azimi S, Mohajerzadeh S, Amini A, Vali A and Mehran M 2010 Realization of three-dimensional micro and nano-structures on silicon substrates *Sci. Iran* **17** 113–21

[29] Moreno M, Daineka D and Roca i Cabarrocas P 2010 Plasma texturing for silicon solar cells: from pyramids to inverted pyramids-like structures *Sol. Energy Mater. Sol. Cells* **94** 733–7

[30] Choi J H, Hwang S M, Lee J Y, Garay A A and Chung C W 2016 Highly anisotropic etching of Ta thin films using high density plasmas of halogen based gases *Vacuum* **133** 18–24

[31] Dai L, Song W, Wang S, Zhong Z and Zhang G 2015 Pressure-dependent etching mechanism and induced dielectric properties variation of BZN thin films in SF_6/Ar plasma *Plasma Chem. Plasma Process.* **35** 1119–27

[32] Azimi S, Mehran M, Amini A, Vali A, Mohajerzadeh S and Fathipour M 2010 Formation of three-dimensional and nanowall structures on silicon using a hydrogen-assisted high aspect ratio etching *J. Vac. Sci. Technol.* B **28** 1125–31

[33] Lee Y, Kim H, Iftiquar S M, Kim S, Kim S, Ahn S, Lee Y J, Dao V A and Yi J 2014 Study of stacked-emitter layer for high efficiency amorphous/crystalline silicon heterojunction solar cells *J. Appl. Phys.* **116** 244506

[34] Kim S, Iftiquar S M, Lee D, Lee H, Kim J, Jung J, Oh D, Dao V A and Yi J 2016 Improvement in front-contact resistance and interface passivation of heterojunction amorphous/crystalline silicon solar cell by hydrogen-diluted stacked emitter *IEEE J. Photovolt.* **6** 837–45

[35] Kim I, Jeong D S, Lee W S, Kim W M, Lee K S and Lee T S 2016 Asymmetric back contact nanograting design for thin c-Si solar cells *Curr. Appl. Phys.* **16** 568–73

[36] Li X, Abe T and Esashi M 2001 Deep reactive ion etching of Pyrex glass using SF_6 plasma *Sensors Actuators* A **87** 139–45

[37] Park J H, Lee N E, Lee J, Park J S and Park H D 2005 Deep dry etching of borosilicate glass using SF_6 and SF_6/Ar inductively coupled plasmas *Microelectron. Eng.* **82** 119–28

[38] Chen Q, Fang J, Ji H F and Varahramyan K 2007 Fabrication of SiO_2 microcantilever using isotropic etching with ICP *IEEE Sensors J.* **7** 1632–8

[39] Plettl A, Enderle F, Saitner M, Manzke A, Pfahler C, Wiedemann S and Ziemann P 2009 Non-close-packed crystals from self-assembled polystyrene spheres by isotropic plasma etching: adding flexibility to colloid lithography *Adv. Funct. Mater.* **19** 3279–84

[40] Laermer F, Franssila S, Sainiemi L and Kolari K 2010 Deep reactive ion etching *Handbook of Silicon Based MEMS Materials and Technologies* (New York: Elsevier) pp 349–74

[41] Iftiquar S M, Jung J and Yi J 2017 Improved efficiency of perovskite-silicon tandem solar cell near the matched optical absorption between the subcells *J. Phys. D: Appl. Phys.* **50** 405501

[42] Perrin J 1991 Plasma and surface reactions during a-Si:H film growth *J. Non-Cryst. Solids* **137–8** 639–44

[43] Abouelsaood A A, El-Naggar S A and Ghannam M Y 2002 Shape and size dependence of the anti-reflective and light-trapping action of periodic grooves *Prog. Photovolt: Res. Appl.* **10** 513–26

[44] Back F, Bockmeyer M, Rudigier-Voigt E and Löbmannb P 2014 Periodic nanostructures imprinted on high-temperature stable sol-gel films by ultraviolet-based nanoimprint lithography for photovoltaic and photonic applications *Thin Solid Films* **562** 274–81

[45] Becker C, Preidel V, Sontheimer T, Klimm C, Rudigier-Voigt E, Bockmeyer M and Rech B 2012 Direct growth of periodic silicon nanostructures on imprinted glass for photovoltaic and photonic applications *Phys. Status Solidi* c **9** 2079–82

[46] Meier M, Paetzold U W, Ghosh M and Van Erven R 2015 Periodic nano-textures enhance efficiency in multi-junction silicon thin-film solar cells *Phys. Status Solidi* a **212** 30–5

[47] Tan H, Moulin E, Si F T, Schüttauf J W, Stuckelberger M, Isabella O, Haug F J, Ballif C, Zeman M and Smets A H M 2015 Highly transparent modulated surface textured front electrodes for high-efficiency multijunction thin-film silicon solar cells *Prog. Photovolt: Res. Appl.* **23** 949–63